Polymer Chemistry

Accepted Manuscript

ROYAL SOCIETY OF CHEMISTRY

www.rsc.org/polymers

Cite this: DOI: 10.1039/c0xx00000x

www.rsc.org/xxxxxx

ARTICLE

Antifouling and antibacterial hydrogel coatings with self-healing properties based on dynamic disulfide exchange reaction

Wen Jing Yang[*a], Xi Tao[a], Tingting Zhao[a], Lixing Weng[b], En-Tang Kang[c] and Lianhui Wang[*a]

Received (in XXX, XXX) Xth XXXXXXXXX 20XX, Accepted Xth XXXXXXXXX 20XX

DOI: 10.1039/b000000x

Multifunctional self-healing hydrogel coatings based on dynamic disulfide exchange reaction were developed *via* surface-initiated thiol-ene photopolymerization. The functional monomers, (poly(ethylene glycol)methyl ether methacrylate (PEGMA), *N*-hydroxyethyl acrylamide (HEAA) and 2-(methacryloyloxy)ethyl trimethylammonium chloride (META)), and disulfide-containing crosslinker bis(2-methacryloyl)oxyethyl disulfide (BMOD) were employed for the preparation of antifouling, antibacterial and self-healing hydrogel coatings. The hydrogel coatings reduced protein adsorption, as well as bacteria adhesion from Gram-negative *Escherichia coli* (*E. coli*). Moreover, the coatings exhibited good self-healing ability at moderate temperatures due to the dynamic disulfide exchange reaction. Introduction of self-healing ability provides a promising means for self-repairing of microcracks of functional polymer coatings and improving their stability and durability in the long-term applications as biomaterials.

Introduction

Polymer coatings have been extensively employed in the surface functionalization of biomaterials and biomedical devices, especially in imparting their surface with antifouling and antibacterial properties.[1-3] However, the occurrence of microcracks is inevitable during long-term application of these polymer coatings, and can lead to the devastation and failure of the devices.[4-6] Accordingly, healing of the microcracks is of great importance in improving the stability and durability of functional polymer coatings in long-term applications. Recently, self-healing materials have attracted considerable interests due to their unique feature of healing/repairing themselves, either spontaneously or in response to environmental stimuli such as heat, light and/or pH changes.[7-11] In comparison to conventional repairing approaches at macroscopic level, such as welding and patching, self-healing polymers can be more effective for microcracks healing in the early stage of damage processes.[4,5] Furthermore, the self-healing coatings are advantageous for applications in the less accessible areas. Thus, they are highly favorable for biomaterials and biomedical devices.

Two main strategies have been employed in designing self-healing materials. The first one is based on an irreversible system containing micro/nano-reservoirs, the cracking of which releases the healing reagents.[12-14] In this case, the materials can only heal once. The other strategy is based on reversible bonding systems.[6,15-18] They are able to heal repeatedly, arising from the dynamic covalent or non-covalent interactions. Various covalent and non-covalent bonds have been explored for construction of reversible self-healing materials.[8,9,17-19] In contrast to the non-covalent system, such as hydrogen bonding,[20] covalent bonds are preferable due to their greater bond strength. In the case of strong covalent interactions, a re-mendable polymeric material was first designed based on thermo-reversible Diels-Alder reaction.[17] However, the healing process usually requires high temperatures as external stimulus for Diels-Alder reaction. Therefore, the reversible weak covalent interactions show greater potential for application in self-healing systems. For reversible weak covalent interaction, disulfide bonds impart the healing functionality through dynamic exchange of disulfide reaction at low temperature with relative strong bonds.[21-24] Furthermore, the disulfide exchange reaction can be carried out under ambient conditions without any external stimuli.[21,22] In addition, the thiol radicals, generated by mechanical breakage of disulfide bonds, can rapidly exchange with other disulfide bonds, preventing catastrophic fractures of the materials.[21] Thus, the disulfide exchange reaction can potentially be used for the construction of self-healing polymer coatings.

In the present work, a simple and versatile strategy for the preparation of multifunctional self-healing hydrogel coatings, based on dynamic disulfide exchange reaction, was developed. The functional hydrogel coatings were synthesized *via* the highly-efficient thiol-ene photopolymerization on the stainless steel surface in a "grafting-through" approach[15] (***Scheme 1***). The crosslinker bis(2-methacryloyl)oxyethyl disulfide (BMOD), containing disulfide bond, was employed for introducing self-healing properties based on the disulfide exchange reaction. In this way, it is relatively easy to prepare self-healing coatings with different functionalities by selection of different functional monomers, especially antifouling and antibacterial coatings for biomaterials and biomedical devices. The functional monomers, poly(ethylene glycol)methyl ether methacrylate (PEGMA), *N*-

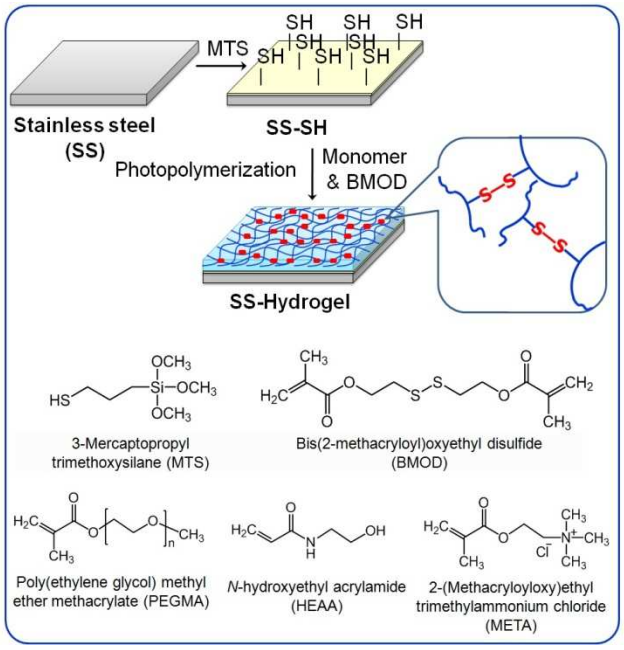

Scheme 1 Schematic illustration of the preparation of hydrogel-functionalized SS surfaces *via* surface-initiated thiol-ene photopolymerization

hydroxyethyl acrylamide (HEAA) and 2-(methacryloyloxy)ethyl trimethylammonium chloride (META), were employed for preparation of antifouling and antibacterial hydrogel coatings. The antifouling and antibacterial efficacy of hydrogel coatings were evaluated by protein adsorption and bacterial adhesion, while their self-healing properties were investigated by optical microscopy and atomic force microscopy (AFM).

Materials and Methods

Materials

AISI type 304 stainless steel (SS) foils of 0.05 mm in thickness were purchased from Goodfellow Ltd., Cambridge, UK. 3-Mercaptopropyl trimethoxysilane (MTS, 95%), poly(ethylene glycol)methyl ether methacrylate (PEGMA, n~9, average molecular weight M_n~500), *N*-hydroxyethyl acrylamide (HEAA, 97%), 2-(methacryloyloxy)ethyl trimethylammonium chloride solution (META, 80 wt% in H_2O), bis(2-methacryloyl)oxyethyl disulfide (BMOD) and fluorescein isothiocynate-conjugated bovine serum albumin (BSA-FITC) were purchased from Sigma-Aldrich Co., St. Louis, MO. HEAA and PEGMA were passed through an inhibitor-removal column (Sigma-Aldrich) and then stored under an argon atmosphere at 4°C. Gram-negative bacterial *Escherichia coli* (*E. coli*, DH5α) was obtained from the American Type Culture Collection, Manassas, VA, USA.

Immobilization of MTS on SS surfaces

SS foils were cut into 1.6×1.6 cm^2 coupons and cleaned ultrasonically for 5 min each with acetone, ethanol and deionized water. The SS coupons were then rinsed thoroughly with deionized water and activated by immersing in piranha solution (H_2SO_4 (95-97%)/H_2O_2 (30%) = 3:1, v:v) for 30 min. They were rinsed thoroughly with deionized water and ethanol, and then dried under a nitrogen stream. Silanization was performed by immersing the SS coupons in ethanol solution of MTS (2.5% w/v) and oscillated at 150 rpm at room temperature for 2 h. Afterwards, the silanized SS substrates (denoted as the SS-SH surfaces) were thermally cured at 110°C for 2 h. The resulting SS-SH substrates were then washed thoroughly with deionized water and stored in a vacuum desiccator after drying under reduced pressure.

Preparation of hydrogel-functionalized SS surfaces *via* surface-initiated thiol-ene photopolymerization

The hydrogel-functionalized SS surfaces were prepared *via* surface-initiated thiol-ene photopolymerization on the SS-SH surfaces in a "grafting-through" approach. BMOD was utilized as a crosslinker in the preparation of hydrogel coatings. For the preparation of antifouling poly(PEGMA) hydrogel-functionalized SS surface (SS-PPEGMA), the SS-SH substrate was introduced into a pyrex glass tube containing 0.45 ml of PEGMA (0.97 mmol), 0.028 ml of BMOD (0.10 mmol) and 2.0 ml of ethanol (crosslinker/monomers molar ratio: 10:100). Then the reaction mixture was degassed for 30 min with nitrogen, followed by exposure to UV irradiation for 1 h under a UV lamp (Spectroline model EN-280L/FA-8W, Spectronics Corporation of New York, USA). For the preparation of antifouling and antibacterial poly(HEAA-*co*-META) hydrogel-functionalized SS surface (SS-P(HEAA-*co*-META)), the SS-SH substrate, 0.17 ml of META (0.71 mmol), 0.07 ml of HEAA (0.71 mmol), 0.036 ml of BMOD (0.14 mmol) and 2.0 ml of ethanol were introduced into a Pyrex glass tube (crosslinker/monomers molar ratio: 10:100). The mixture was degassed and then exposed to UV irradiation for 1 h. The final SS coupons were soaked in ethanol and deionized water for 24 h. The solvent was changed every 3 h to remove the unreacted chemicals. Meanwhile, the free hydrogels (PPEGMA and P(HEAA-*co*-META)) were prepared *via* the same synthesis approach for mechanical characterization purpose. In addition, two kinds of hydrogel coatings on SS substrates were also prepared by using different molar ratios between crosslinker and monomers. The resulted surfaces were denoted as SS-PEGMA-C1 and SS-P(HEAA-*co*-META)-C1 for crosslinker/monomers molar ratio of 1:100, and SS-PEGMA-C100 and SS-P(HEAA-*co*-META)-C100, for crosslinker/monomers molar ratio of 100:100, respectively .

Surface characterization

Static water contact angles (CA) of the piranha solution treated SS substrates, SS-SH surfaces and hydrogel-functionalized SS surfaces were measured at room temperature with a DSA 20 contact angle analyzer (Kruss GmbH Co., Germany), using the sessile drop method with a 3 µl water droplet. At least three measurements were made on each sample to obtain the average value. The chemical composition of functionalized SS substrates was determined by X-ray photoelectron spectroscopy (XPS). XPS measurements were carried out on a Kratos AXIS Ultra spectrometer with a monochromatized Al Kα X-ray source (1486.6 eV photons), at a constant dwelling time of 100 ms and pass energy of 40 eV. The core-level signals were obtained at a photoelectron take-off angle (α, with respect to the sample surface) of 90°. All binding energies (BEs) were referenced to the neutral C 1s hydrocarbon peak at 284.6 eV. The topographies of the thiol- and hydrogel-functionalized surfaces were studied on

glass substrates by atomic force microscope (AFM, Dimension icon, Bruker, Germany). The root mean square (RMS) roughnesses (R_q) were calculated from the roughness profile.

Hydrogel characterization

The gel fractions and equilibrium water swelling ratios were measured gravimetrically.[25,26] The as-prepared free hydrogels were dried in a vacuum oven at 60°C to a constant weight (W_i), and then subjected to ethanol and deionized water extraction for 48 h at room temperature. The extracted hydrogels were dried again in a vacuum oven at 60°C to a constant weight (W_d). The gel fractions (GF) were calculated as follows: $GF=W_d/W_i$, where W_d is the weight of the dried insoluble part of sample after extraction with ethanol and water, while W_i is the initial dry hydrogel. The equilibrium water swelling ratios (ESR) were calculated as follows: $ESR=(W_s - W_d)/W_d$, where W_d and W_s represent the weights of dry and equilibrium swollen hydrogels.

The mechanical measurements of the free hydrogels were carried out using a universal testing machine (CMT5305, SUST Electrical Equipment Co., LTD). All the hydrogel samples were prepared in cylindrical shape with an 8 mm diameter and 15 mm height. The stress-strain measurements were taken at a compression rate of 2 mm min^{-1}. Compressive modulus was then determined as the slope at the 0-10% strain range from the stress-strain curve[27].

Protein adsoprption assays

Adsorption of BSA-FITC on the hydrogel-functionalized SS surfaces was examined with a fluorescence microscope. The functionalized SS substrates were rinsed initially with a normal saline (NS) solution and then placed in the BSA-FITC solution (1 mg ml^{-1} NS solution) at room temperature for 1 h. The substrates were gently rinsed with NS solution and the adsorption was imaged under inverted fluorescence microscope (Nikon, eclipse Ti-U, Japan). The fluorescence intensity, which was proportional to the surface density of adsorbed BSA-FITC protein, was quantified using the ImageJ software (National Institutes of Health, Bethesda, MD, USA).

Antibacterial assays

Gram-negative bacterial *Escherichia coli* (*E. coli*, DH5α) was used for the evaluation of the anti-bacterial adhesion characteristics and bactericidal efficacy of the hydrogel-functionalized surfaces. *E. coli* was cultured in the nutrient broth at 37°C overnight. After incubation, the bacterial suspension was centrifuged at 6000 rpm for 3 min. Upon removal of the supernatant, the bacterial cells were washed with NS solution twice and resuspended in NS solution at a concentration of 5×10^7 cells ml^{-1}. Each substrate was immersed in the bacterial suspension under static condition at 37°C for 4 h. After fixing with 3% glutaraldehyde and dehydrating with serial ethanol, the adhered bacterial cells were investigated under a scanning electron microscope (SEM, Model S-4800, Hitachi Co., Tokyo, Japan). Quantification of bacterial adhesion and viability on the uncoated and hydrogel-functionalized SS was carried out by the spread plate method.[28] The result was expressed as a viable adherent fraction, which is defined as the percentage of viable adherent bacteria cells on the hydrogel-functionalized SS surface relative to those on the uncoated SS surface.

Self-healing assays

Studies of the self-healing behavior of the hydrogel coatings on glass substrates were conducted using a step profiler (Dektak XT, Bruker, Germany) and atomic force microscopy (AFM). Firstly, scratches were created on the thick hydrogel coatings (thickness>10 μm) by the probe of step profiler, followed by observation using the optical microscope of step profiler *in situ*. Secondly, the thin hydrogel coatings (about 390 nm) were damaged using a razor blade. The topographic changes were observed under an optical microscope and AFM.

Results and Discussions

Multifunctional hydrogel-functionalized SS surfaces

The procedures for preparation of multifunctional hydrogel coatings on stainless steel (SS) surfaces are shown in ***Scheme 1***. 3-Mercaptopropyl trimethoxysilane (MTS) was first coated on the SS surface to introduce the thiol groups for subsequent surface-initiated thiol-ene photopolymerization. Due to its high polymerization rate and conversion efficiency, the thiol-ene photopolymerization has been considered as "click chemistry" and widely used in the production of surface-grafted polymer films.[29,30] Bis(2-methacryloyl)oxyethyl disulfide (BMOD) containing disulfide bond was utilized as a crosslinker and for the introduction of self-healing properties based on dynamic disulfide exchange reaction. Three functional monomers, poly(ethylene glycol)methyl ether methacrylate (PEGMA), *N*-hydroxyethyl acrylamide (HEAA) and 2-(methacryloyloxy)ethyl trimethylammonium chloride (META), were employed for imparting antifouling and antibacterial properties. Two hydrogel-functionalized SS surfaces were synthesized, including bifunctional (antifouling and self-healing) poly(PEGMA)-functionalized surface (SS-PPEGMA) and multifunctional (antifouling, antibacterial and self-healing) poly(HEAA-*co*-META)-functionalized surface (SS-P(HEAA-*co*-META)). The disulfide bonds, introduced by the crosslinker, can undergo reversible disulfide exchange reaction once the cracks occur, as shown in ***Scheme 2***. Through the dynamic disulfide exchange reaction process, the hydrogel coatings are expected to self-heal under room temperature, even without any catalysts.

Table 1 shows the static water contact angles of the functionalized SS surfaces. The static water contact angle of the thiol-functionalized SS surface (SS-SH) is 73±3°, much higher than that of piranha solution treated SS surface (denoted as uncoated SS surface: 27±3°). For the hydrogel coatings, the water contact angles decreased greatly, with respective water contact angels of 46±2° and 31±3° for the poly(PEGMA) and poly(HEAA-*co*-META) hydrogel coatings. The decrease in the water contact angles is consistent with the hydrophilic nature of hydrogel coatings on the SS surfaces. Apart from the measurement of water contact angles, the chemical composition

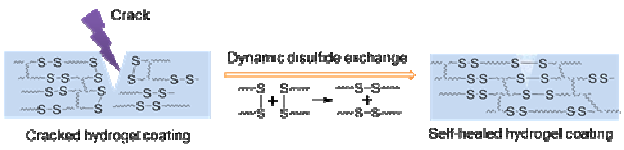

Scheme 2 Schematic illustration of the self-healing process of hydrogel coatings based on disulfide exchange reaction

Table 1 Static water contact angles and surface composition of the hydrogel-functionalized stainless steel (SS) surfaces

Surfaces	Static water contact angle (mean ± SD[a], Degrees)	Surface composition[b] (molar ratio)
Uncoated SS[c]	27±3	-
SS-SH	73±3	[C]:[Si]:[S]=32.5:4.1:1
SS-PPEGMA	46±2	[C]:[O]:[S]=58.2:23.5:1
SS-P(HEAA-*co*-META)	31±3	[C]:[N]:[Cl]:[S]=103:6.5:4.2:1

[a] SD: Standard deviation; [b] Determined from XPS analysis; [c] Uncoated SS: SS treated with piranha solution

of uncoated and functionalized SS surfaces was analyzed by X-ray photoelectron spectroscopy (XPS). For the uncoated SS surface, only C 1s and O 1s signals, with binding energies (BEs) about 285 eV and 532 eV, respectively, can be observed in the wide scan spectrum (Fig. 1a), indicating the presence of residual organic contaminants on the uncoated SS surface.[31] After silanation with MTS, several additional signals appear in the wide scan spectrum of SS-SH surface (Fig. 1b), including S (2s: 228 eV, 2p: 164 eV) and Si (2s: 151 eV, 2p: 99 eV) XPS peaks.[32,33] The appearance of these signals indicates the successful introduction of thiol groups on the SS surfaces for the subsequent surface-initiated thiol-ene photopolymerization.

The antifouling and self-healing SS-PPEGMA surface was synthesized by photopolymerization of PEGMA and BMOD crosslinker. The Si 2s and 2p core-level signals, with respective BEs of 151 eV and 99 eV, have disappeared completely in the wide scan spectrum of SS-PPEGMA surface (Fig. 1c), suggesting a dense layer of PPEGMA coating has been synthesized on the surface. The XPS C 1s core-level spectrum of SS-PPEGMA surface (Fig. 1d) consists of three peak components with BEs at 284.6 eV, 286.2 eV and 288.5 eV, attributable to the *C*-H, *C*-O and O-*C*=O species, respectively.[32,34] The high content of *C*-O species is consistent with the successful photopolymerization of PEGMA from the surface.

For the multifunctional (antifouling, antibacterial and self-healing) SS-P(HEAA-*co*-META) surface, the appearance of the nitrogen and chlorine signals (N 1s: 399 eV, Cl 2s: 271 eV, Cl 2p: 199 eV) in the wide scan spectrum (Fig. 1e), are consistent with the presence of poly(HEAA-*co*-META) hydrogel coating after photopolymerization. The corresponding C 1s core-level spectrum (Fig. 1f) can be curve-fitted into five peak components with BEs at 284.6 eV, 285.6 eV, 286.3 eV, 287.2 eV and 288.7 eV, attributable to *C*-H, *C*-N, *C*-O/*C*-S, HN-*C*=O and O-*C*=O species, respectively.[32] The N 1s core-level spectrum (Fig. 1g) comprises of two peak components with BEs at of 399.7 eV and 402.7 eV, corresponding to the amine (C-*N*) and quaternary ammonium cationic (-*N*$(CH_3)_3^+$) species, respectively.[32,35] The XPS S 2p core-level spectrum (Fig. 1h) consists of a spin-orbit split doublet, with the BEs of S $2p_{3/2}$ and S $2p_{1/2}$ peak components at 163.1 and 164.3 eV, respectively, attributable to the covalently bonded sulfur (C-*S*) species.[32]

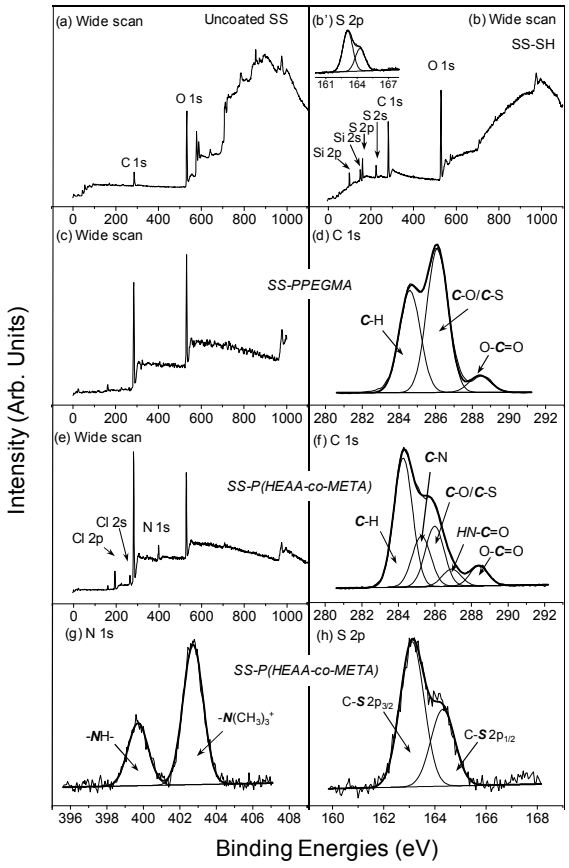

Fig. 1 (a) XPS wide scan spectrum of the uncoated SS surface, (b and b') XPS wide scan and S 2p core-level spectra (inset) of the SS-SH surface, (c and d) XPS wide scan and C 1s core-level spectra of the SS-PPEGMA surface, (e-h) XPS wide scan, C 1s, N 1s and S 2p core-level spectra of the SS-P(HEAA-*co*-META) surface

Surface morphologies of the functionalized SS surfaces

The morphologies of hydrogel-functionalized SS surfaces were investigated by atomic force microscope (AFM), as shown in Fig.

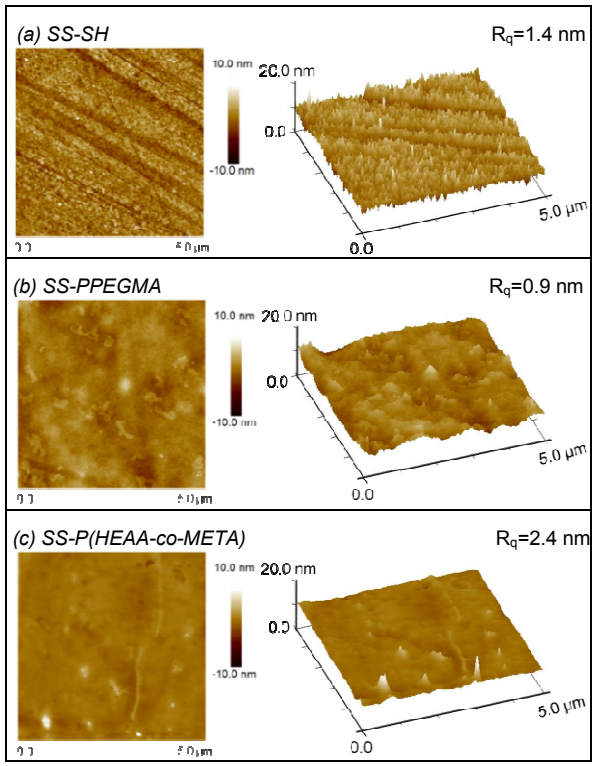

Fig. 2 Atomic force microscopy (AFM) images of the (a) SS-SH, (b) SS-PPEGMA, (c) SS-P(HEAA-*co*-META) surfaces. R_q= Root-mean-square roughness

2. All the functionalized SS surfaces exhibit a homogeneous and uniform topography, with surface root-mean-square (RMS) roughness (R_q) of 0.9~2.4 nm over an area of 5×5 μm^2. The SS-SH surface shows a RMS roughness with 1.4 nm (Fig. 2a). As for the SS-PPEGMA and SS-P(HEAA-*co*-META) surfaces, dense and uniform hydrogel coatings were grafted from the SS-SH surfaces, with respective RMS roughness of 0.9 and 2.4 nm (Fig. 2b and c).

Hydrogel characterizations

Apart from characterization of the hydrogel coatings on SS substrates, the physical parameters, such as gel fraction and equilibrium water swelling ratio, of the free hydrogels were also measured. The gel fractions of the PPEGMA and P(HEAA-*co*-META) hydrogels are 42.5% and 66.3%, respectively, indicating a higher degree of crosslinking in the P(HEAA-*co*-META) hydrogel. Furthermore, the water swelling ratios are 10.6 and 18.9, respectively, for the PPEGMA and P(HEAA-*co*-META) hydrogels. The mechanical strength of the hydrogels is of great importance for their biomedical applications. Representative compression stress-strain curves of the free hydrogels were shown in Fig. 3. Both the PPEGMA and P(HEAA-*co*-META) hydrogels showed linear stress-strain curves at the initial period, indicative of elastic responses. In comparison to the PPGEMA hydrogel with compressive modulus of 38.6 kPa, the P(HEAA-*co*-META) exhibited a lower modulus of 23.7 kPa.

Protein adsorption on the hydrogel-functionalized SS surfaces

Protein adsorption and fouling are closely related to surface composition.[36,37] Bovine serum albumin (BSA) was selected as the model protein due to its well-known strong adsorption characteristics on many types of materials. The adsorption of fluorescein isothiocynate-conjugated bovine serum albumin (BSA-FITC) on the functionalized SS surfaces was investigated under fluorescence microscope. Fig. 4 shows the fluorescence microscope images and average fluorescence intensities of the hydrogel-functionalized SS surfaces after exposure to 1.0 mg ml^{-1} of BSA-FITC solution for 1 h. As expected, the uncoated SS surface was covered with a large concentration of BSA, as evidenced by the high fluorescence intensity. The result indicates the vulnerability of the uncoated SS surface to protein fouling. In comparison to the uncoated SS surface, the fluorescence intensity of adsorbed BSA on the SS-PPEGMA surface was significantly reduced. The intensity was only about 6% of that of the uncoated SS surface. The resistance to protein adsorption is attributed to

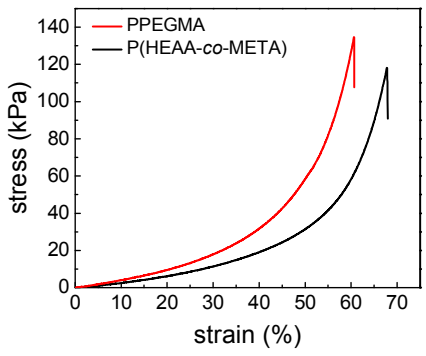

Fig. 3 The compressive stress-strain curves of the free hydrogels

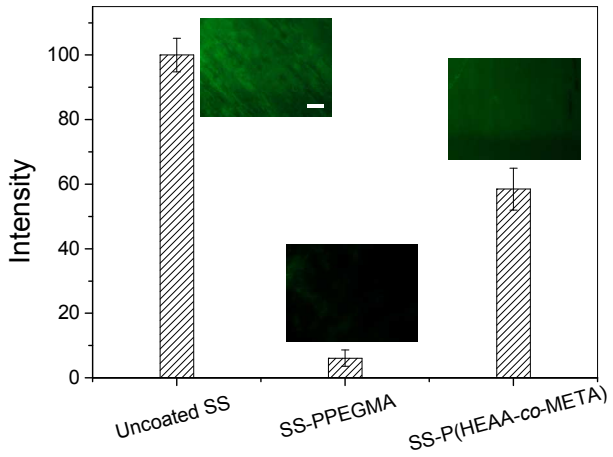

Fig. 4 Fluorescence microscope images of the uncoated SS, SS-PPEGMA and SS-P(HEAA-*co*-META) surfaces after exposure to BSA-FITC solution. (Scale bar: 100 μm)

the repulsive hydrodynamic forces arising from strong solvation of the hydrophilic poly(PEGMA) surface.[38,39] As for the SS-P(HEAA-*co*-META) surface, the fluorescence intensity was reduced to 59% of that on the uncoated SS surface, indicating its good resistance to protein adsorption. The SS-P(HEAA-*co*-META) surface exhibits lower resistance to BSA adsorption than the SS-PPEGMA surface. The phenomenon probably has resulted from the electrostatic interaction of the negatively charged BSA protein with the positive terminal groups in the poly(META) components.[40] As for the SS-PEGMA-C1 and SS-PEGMA-C100 surfaces, the resistances to protein adsorption were comparable on both surfaces, about 55% of the uncoated SS surface, as shown in Fig. S1. The other two surfaces, SS-P(HEAA-*co*-META)-C1 and P(HEAA-*co*-META)-C100, also reduced protein adsorption (Fig. S1).

Bacterial-fouling assays of the hydrogel-functionalized SS surfaces

The antimicrobial activities of the hydrogel-functionalized SS surfaces were evaluated by Gram-negative *Escherichia coli (E. coli)*. Fig. 5 shows the scanning electron microscope (SEM) images of uncoated SS and hydrogel-functionalized SS surfaces after bacterial fouling. The uncoated SS surface is highly susceptible to adhesion and colonization of bacteria, as evidenced by the large amount of bacterial cells on the SS surface, either individually or in small clusters (Fig. 5a). For the SS-PPEGMA surface, a significant reduction in bacterial adhesion was observed. Only a few bacteria cells were found to be distributed sparsely on the SS-PPEGMA surface (Fig. 5b). A few bacteria cells were also observed on the SS-P(HEAA-*co*-META) surface (Fig. 5c). However, the morphologies of bacterial cells are quite different from that of the bacterial cells on the uncoated SS surface. Apart from distorted and wrinkled membranes, lesions and holes were also observed in bacterial cells on the SS-P(HEAA-*co*-META) surface. Similar phenomenon was also observed on other polycationic hydrogel surfaces, as they were like an "anion sponge" leading to microbial membrane disruption and then microbe death.[41,42] The hydrogel coatings prepared by different molar ratio of crosslinker and monomers were also

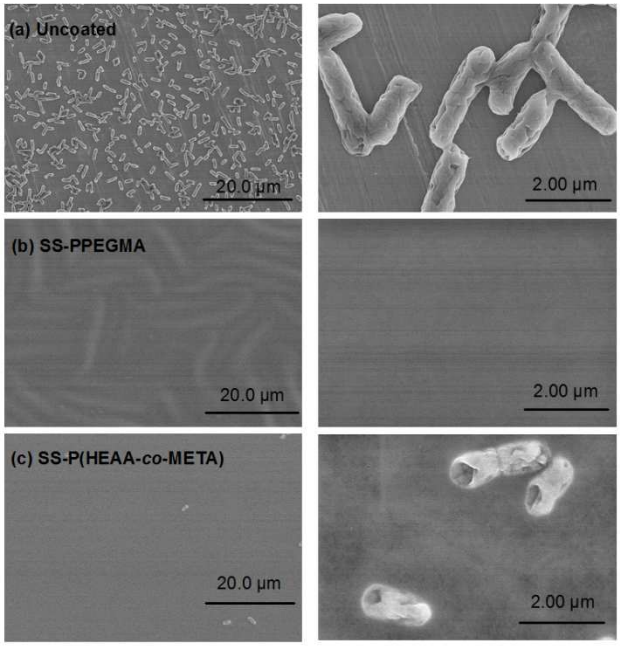

Fig. 5 Scanning electron microscopy (SEM) images of the (a) uncoated SS, (b) SS-PPEGMA, (c) SS-P(HEAA-*co*-META) surfaces after exposure to *E. coli* (5×10^7 cells ml^{-1}) for 4 h

tested in the bacterial fouling assays (Fig. S2). As shown in Fig. S2b and d, the morphology of the underlying SS substrates can be observed for SS-PPEGMA-C1 and SS-P(HEAA-*co*-META)-C1 surfaces, indicating very thin hydrogel coatings were obtained using less crosslinker. For the SS-PPEGMA-C100 and SS-P(HEAA-*co*-META)-C100 surfaces (Fig. S2c and e), rough and dense coatings were observed, probably caused by the inhomogeneity generated in the hydrogel preparation using high crosslinker content.[43] All the SS-PPEGMA and SS-P(HEAA-*co*-META) surfaces, prepared by using crosslinker/monomers ratio of 1:100 and 100:100 (Fig. S2b'-e'), exhibited lower antibacterial efficiency in comparison to those of 10:100 (Fig. 5b and c).

A more quantitative antibacterial assay was carried out using the spread plate method. Fig. 6 shows the viable adherent fractions of *E. coli* on the uncoated and hydrogel-functionalized SS surfaces after 4 h of exposure to the bacterial suspension. In comparison to the uncoated SS surface, both the hydrogel-

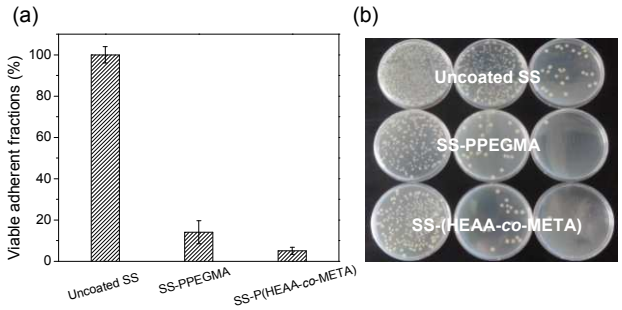

Fig. 6 (a) Viable adherent fractions of *E. coli* on the uncoated, SS-PPEGMA and SS-P(HEAA-*co*-META) surfaces after exposure to same bacterial solution of *E. coli* (5×10^7 cells ml^{-1}) for 4 h. (b) Images of *E. coli* colonies of the viable adherent bacterial cells on the uncoated (upper), SS-PPEGMA (middle) and SS-P(HEAA-*co*-META) (lower) surfaces after spread on agar plate. The decrease colony counts from left to right were due to 10-fold diluted bacterial solutions that were spread on agar plates.

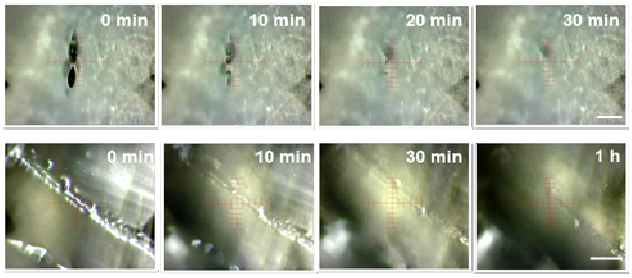

Fig. 7 Self-healing behavior of the hydrogel coatings under optical microscope of step profiler. The scratch/cut was performed by the tip of step profiler. Scale bar: 220 μm. (Upper: SS-PPEGMA, Lower: SS-P(HEAA-*co*-META))

functionalized SS surfaces exhibited above 86% reduction of bacterial adhesion. The multifunctional SS-P(HEAA-*co*-META) surface exhibited higher antibacterial efficiency than the bifunctional SS-PPEGMA surface, with adherent viable fractions of 5% and 14%, respectively. The poly(PEGMA) hydrogel coating resists bacterial adhesion *via* the strong hydration of PEG units in the side chains of the hydrogel. In comparison to the poly(PEGMA) coating, the poly(HEAA-*co*-META) hydrogel coating not only resists bacterial adhesion, but also exhibits bactericidal effect. More specifically, the poly(META) components in the hydrogel coating could disrupt cell membranes through the actions of quaternary ammonium cations, while the poly(HEAA) components could become highly hydrated to resist bacterial adhesion due to two hydrogen-bond donors from the hydroxyl (-OH) and amide (-NH-) groups in the side chain. The high antifouling and antimicrobial efficacies of the hydrogel-functionalized SS surfaces are thus ascertained by the SEM images as well as the bacterial fouling assays.

Self-healing behavior of the hydrogel coatings

The self-healing behavior of the hydrogel-functionalized SS surfaces was monitored by the optical microscope and AFM. Fig. 7 shows the self-healing behavior of the two hydrogel coatings (above 10 μm in thickness) in 30-60 min. After damages on coatings were induced by the probe of step profiler, the topographical changes were monitored by optical microscope of step profiler *in situ*. For the poly(PEGMA) hydrogel coating, a small damaged area was induced by the probe. The initial scratch disappeared in 30 min, returning the surface with uniform coating. Subsequently, a cut of about 50 μm in width was made on the poly(HEAA-*co*-META) hydrogel coating. After 30 min, the extent of damage decreased substantially, and the damaged area healed almost fully after 1 h. The healing process occurred spontaneously at room temperature without any external stimulus. This quick healing-response can be attributed to the large thickness of the hydrogel coatings. It has been observed that the thicker films can heal from wider cuts, as the droop caused by higher surface tension can provide contact between the damaged surfaces and then triggers the healing process.[21]

The self-healing processes from microscopic cuts (about 10 μm in width) on thinner hydrogel coating (about 390 nm for the SS-P(HEAA-*co*-META) surfaces), were monitored by the optical microscope of AFM for 72 hours. In Fig. 8, the lumps at the edge of the cut were the polymer debris that was generated during the scratch.[44] The scratch was healed initially from the narrower parts

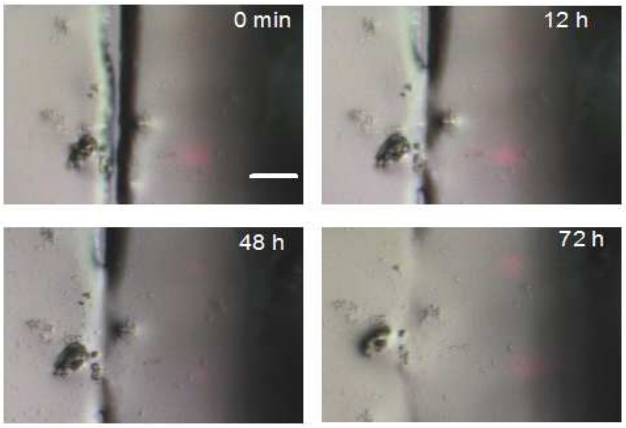

Fig. 8 Self-healing behaviour of the hydrogel coatings under the optical microscope of AFM. The scratch was performed by a blade. (Scale bar: 50 μm)

to the scratch. After 12 hours, the scratched area had healed partially. A more complete healing was achieved in 48 hours. As a common principle for the self-healing process, the generation of "mobile phase" is indispensible.[45] The subsequent repairing process includes the directed mass transport and subsequent local mending reaction based on physical interactions or chemical bonds. In order to improve the generation of the "mobile phase", a drop of water was sprayed on the small unhealed area of the cut and the coating was set still at room temperature for another 24 hours. As a result, the hydrogel coating had recovered almost completely and exhibited a uniform surface, indicating the importance of the phase mobility. In this case, the healing action was trigged by the disulfide exchange reaction after the "mobile phase" was generated. More specifically, the disulfide bonds in the "mobile phase" at the cut interface can exchange with other disulfide bonds to accomplish the rebonding. On the other hand, the thiyl radicals, produced from the mechanical breakage of disulfide bonds, are also expected to be exchanged rapidly with other disulfide bonds.[21] In comparison to the hydrogel coatings prepared using crosslinker/monomers molar ratio of 10:100, the other hydrogel coatings, prepared by the ratio of 1:100 and 100:100, cannot self-heal from scratches under the same external conditions (Fig. S3).

Furthermore, the self-healing process of a cut with width less than 10 μm in the multifunctional hydrogel coating (poly(HEAA-*co*-META)) was observed by AFM, as shown in Fig. 9a. A scratch with width of around 7.8 μm was created by a blade on the dry hydrogel coating surface (Fig. 9a(1)). Similarly, a trace amount of water was dripped to create the "mobile phase". After 12 hours, the cut size decreased from 7.8 μm to 4.2 μm in width (Fig. 9a(2)). After repeating the process, a completely healed coating with smooth surface was observed (Fig. 9a(3)). Therefore, the self-healing properties of the multifunctional hydrogel coating have been ascertained.

In addition, the antibacterial performances of the cracked hydrogel coating were also explored. Fig. 9b shows SEM images of scratched hydrogel coating before and after bacterial fouling for 4 h. A few bacterial cells were present on the partially healed hydrogel coating, as comparable with that of the undamaged ones (Fig. 5c). It indicates that the multifunctional hydrogel coating is effective in resisting bacterial fouling even with scratches initially.

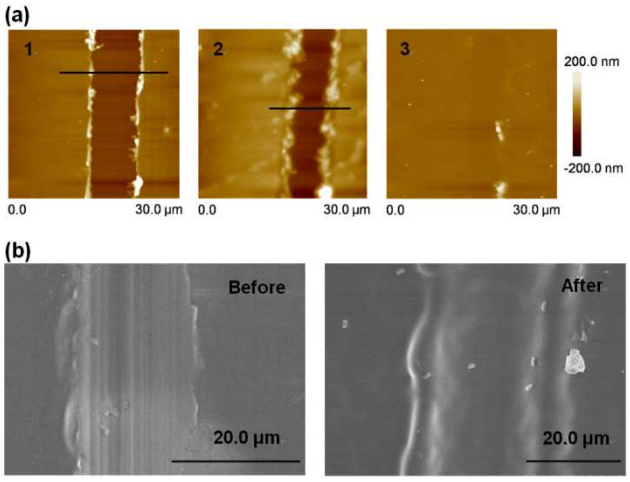

Fig. 9 (a) Self-healing behavior of the hydrogel coating under the atomic force microscopy (AFM). 1. The scratched hydrogel coating (cut width: 7.8 μm); 2. partially healed hydrogel coating after sprinkle of a trace amount of water at 37°C for 12 h (cut width: 4.2 μm); 3. healed hydrogel coating by repeating the process (sprinkle a trace amount of water at 37°C for 12 h). (b) SEM images of the scratched hydrogel coating before and after exposure to E. coli (5×107 cells ml^{-1}) suspension for 4 h

Conclusions

The multifunctional hydrogel coatings were prepared *via* the highly-efficient thiol-ene photopolymerization of the functional monomers (poly(ethylene glycol)methyl ether methacrylate (PEGMA), *N*-hydroxyethyl acrylamide (HEAA) and 2-(methacryloyloxy)ethyl trimethylammonium chloride (META)) and disulfide-containing crosslinker bis(2-methacryloyl)oxyethyl disulfide (BMOD). By employing the reversible disulfide exchange reactions, self-healing properties were introduced into the antifouling and antibacterial hydrogel coatings. Both of the self-healing hydrogel coatings (poly(PEGMA) and poly(HEAA-*co*-META)) reduced bovine serum albumin adsorption significantly. As for the adhesion of Gram-negative bacterial *E. coli*, the bacterial adhesion was reduced by above 86% on both hydrogel coatings. In addition, the hydrogel coatings exhibit good self-healing ability at moderate temperatures due to the reversible disulfide exchange reaction. The surface-initiated thiol-ene photopolymerization, employing the disulfide-containing crosslinker, provides a facile and versatile method for preparation of multifunctional self-healing polymer coatings. The as-prepared multifunctional self-healing hydrogels have great potential as an effective and durable coating in long-term applications for biomaterials.

Acknowledgement

The authors would like to acknowledge the financial support of this study from National Key Basic Research Program of China (973) (2012CB933301), National Natural Science Foundation of China Program (21404058), Natural Science Foundation of Jiangsu Province (BK20140864), Program for Changjiang Scholars and Innovative Research Team in University (IRT1148), Sci-tech Support Plan of Jiangsu Province (BE2014719), Priority Academic Program Development of Jiangsu Higher Education Institutions (PAPD), Natural Science Foundation of Universities

from Jiangsu Province (14KJB150017) and NUPTSF (NY213101).

[a] *Key Laboratory for Organic Electronics and Information Displays, Institute of Advanced Materials (IAM), Jiangsu National Synergistic Innovation Center for Advanced Materials (SICAM), Nanjing University of Posts & Telecommunications, 9 Wenyuan Road, Nanjing, 210023, China. E-mail: iamwjyang@njupt.edu.cn; iamlhwang@njupt.edu.cn*
[b] *College of Geography and Biological Information, Nanjing University of Posts and Telecommunications, 9 Wenyuan Road, Nanjing, 210023, China*
[c] *Department of Chemical & Biomolecular Engineering, National University of Singapore, Kent Ridge, Singapore, 119260.*

References

1. K. G. Neoh, X. F. Hu, D. Zheng and E. T. Kang, *Biomaterials*, 2012, **33**, 2813.
2. N. Ayres, *Polym Chem*, 2010, **1**, 769.
3. P. Zhang, J. Yang, W. Li, W. Wang, C. Liu, M. Griffith and W. Liu, *J Mater Chem*, 2011, **21**, 7755.
4. S. Burattini, B. W. Greenland, D. Chappell, H. M. Colquhoun and W. Hayes, *Chem Soc Rev*, 2010, **39**, 1973.
5. D. Y. Wu, S. Meure and D. Solomon, *Prog Polym Sci*, 2008, **33**, 479.
6. Y. Yang and M. W. Urban, *Chem Soc Rev*, 2013, **42**, 7446.
7. S. R. White, N. R. Sottos, P. H. Geubelle, J. S. Moore, M. R. Kessler, S. R. Sriram, E. N. Brown and S. Viswanathan, *Nature*, 2001, **409**, 794.
8. R. J. Wojtecki, M. A. Meador and S. J. Rowan, *Nat Mater*, 2011, **10**, 14.
9. H. Ying, Y. Zhang and J. Cheng, *Nat Commun*, 2014, **5**, 3218.
10. Z. Wei, J. He, T. Liang, H. Oh, J. Athas, Z. Tong, C. Wang and Z. Nie, *Polym Chem*, 2013, **4**, 4601.
11. S. R. White, J. S. Moore, N. R. Sottos, B. P. Krull, W. A. S. Cruz and R. C. R. Gergely, *Science*, 2014, **344**, 620.
12. K. S. Toohey, N. R. Sottos, J. A. Lewis, J. S. Moore and S. R. White, *Nat Mater*, 2007, **6**, 581.
13. C. J. Hansen, W. Wu, K. S. Toohey, N. R. Sottos, S. R. White and J. A. Lewis, *Adv Mater*, 2009, **21**, 4143.
14. Z. L. Zheng, X. Huang, M. Schenderlein, D. Borisova, R. Cao, H. Mohwald and D. Shchukin, *Adv Funct Mater*, 2013, **23**, 3307.
15. M. Henze, D. Madge, O. Prucker and J. Ruhe, *Macromolecules*, 2014, **47**, 2929.
16. M. Krogsgaard, M. A. Behrens, J. S. Pedersen and H. Birkedal, *Biomacromolecules*, 2013, **14**, 297.
17. X. X. Chen, M. A. Dam, K. Ono, A. Mal, H. B. Shen, S. R. Nutt, K. Sheran and F. Wudl, *Science*, 2002, **295**, 1698.
18. M. Nakahata, Y. Takashima, H. Yamaguchi and A. Harada, *Nat Commun*, 2011, **2**, 511.
19. G. H. Deng, C. M. Tang, F. Y. Li, H. F. Jiang and Y. M. Chen, *Macromolecules*, 2010, **43**, 1191.
20. Y. L. Chen, A. M. Kushner, G. A. Williams and Z. B. Guan, *Nat Chem*, 2012, **4**, 467.
21. J. A. Yoon, J. Kamada, K. Koynov, J. Mohin, R. Nicolay, Y. Z. Zhang, A. C. Balazs, T. Kowalewski and K. Matyjaszewski, *Macromolecules*, 2012, **45**, 142.
22. J. Canadell, H. Goossens and B. Klumperman, *Macromolecules*, 2011, **44**, 2536.
23. Z. Q. Lei, H. P. Xiang, Y. J. Yuan, M. Z. Rong and M. Q. Zhang, *Chem Mater*, 2014, **26**, 2038.
24. Mark Pepels, Ivo Filot, Bert Klumperman and H. Goossens, *Polym Chem*, 2013, **4**, 4955.
25. C. S. Biswas, V. K. Patel, N. K. Vishwakarma, A. K. Mishra, S. Saha and B. Ray, *Langmuir*, 2010, **26**, 6775.
26. C. Ghobril and M. W. Grinstaff, *Chem Soc Rev*, 2015, **44**, 1820.
27. B. G. Yang, C. Y. Wang, Y. B. Zhang, L. Ye, Y. F. Qian, Y. Shu, J. M. Wang, J. J. Li and F. L. Yao, *Polym Chem*, 2015, **6**, 3431.
28. W. J. Yang, T. Cai, K. G. Neoh, E. T. Kang, G. H. Dickinson, S. L. M. Teo and D. Rittschof, *Langmuir*, 2011, **27**, 7065.
29. C. E. Hoyle and C. N. Bowman, *Angew Chem Int Edit*, 2010, **49**, 1540.
30. W. J. Yang, K. G. Neoh, E. T. Kang, S. L. M. Teo and D. Rittschof, *Polym Chem*, 2013, **4**, 3105.
31. W. J. Yang, K. G. Neoh, E. T. Kang, S. S. C. Lee, S. L. M. Teo and D. Rittschof, *Biofouling*, 2012, **28**, 895.
32. J. F. Moulder, W. F. Stickle, P. E. Sobol and K. D. Bomben, *Handbook of X-ray photoelectron spectroscopy*, Eden Prarie (MN), 1992.
33. F. Zhang, Z. L. Shi, P. H. Chua, E. T. Kang and K. G. Neoh, *Ind Eng Chem Res*, 2007, **46**, 9077.
34. S. J. Yuan, D. Wan, B. Liang, S. O. Pehkonen, Y. P. Ting, K. G. Neoh and E. T. Kang, *Langmuir*, 2011, **27**, 2761.
35. W. J. Yang, T. Cai, K. G. Neoh, E. T. Kang, S. L. M. Teo and D. Rittschof, *Biomacromolecules*, 2013, **14**, 2041.
36. A. Sethuraman, M. Han, R. S. Kane and G. Belfort, *Langmuir*, 2004, **20**, 7779.
37. Y. Xu, M. Takai and K. Ishihara, *Biomaterials*, 2009, **30**, 4930.
38. F. J. Xu, K. G. Neoh and E. T. Kang, *Prog Polym Sci*, 2009, **34**, 719.
39. H. W. Ma, J. H. Hyun, P. Stiller and A. Chilkoti, *Adv Mater*, 2004, **16**, 338.
40. C. Y. Ba, D. A. Ladner and J. Economy, *J Membrane Sci*, 2010, **347**, 250.
41. P. Li, Y. F. Poon, W. F. Li, H. Y. Zhu, S. H. Yeap, Y. Cao, X. B. Qi, C. C. Zhou, M. Lamrani, R. W. Beuerman, E. T. Kang, Y. G. Mu, C. M. Li, M. W. Chang, S. S. J. Leong and M. B. Chan-Park, *Nat Mater*, 2011, **10**, 149.
42. M. Mizutani, E. F. Palermo, L. M. Thoma, K. Satoh, M. Kamigaito and K. Kuroda, *Biomacromolecules*, 2012, **13**, 1554.
43. B. Lindemann, U. P. Schroder and W. Oppermann, *Macromolecules*, 1997, **30**, 4073.
44. B. C. Allison, B. M. Applegate and J. P. Youngblood, *Biomacromolecules*, 2007, **8**, 2995.
45. T. Lan, W. J. Yang, J. Peng, M. K. Li and Y. H. Wang, *Polym Int*, 2014, **63**, 1691.

TOC Graphic

Title: Antifouling and Antibacterial Hydrogel Coatings with Self-healing Properties based on Dynamic Disulfide Exchange Reaction

Authors: Wen Jing Yang[*a], Xi Tao[a], Tingting Zhao[a], Lixing Weng[b], En-Tang Kang[c] and Lianhui Wang[*a]

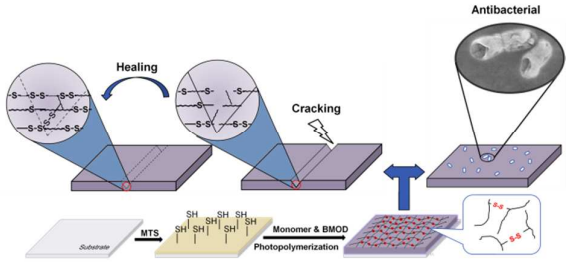

Antifouling and antibacterial hydrogel coatings with self-healing properties were developed *via* simple surface-initiated thiol-ene photopolymerization.